Molecules and Cells

Lipofuscin Granule Accumulation Requires Autophagy Activation

Seon Beom Song, Woosung Shim, and Eun Seong Hwang*

Department of Life Science, University of Seoul, Seoul 02504, Korea
*Correspondence: eshwang@uos.ac.kr
https://doi.org/10.14348/molcells.2023.0019
www.molcells.org

Lipofuscins are oxidized lipid and protein complexes that accumulate during cellular senescence and tissue aging, regarded as markers for cellular oxidative damage, tissue aging, and certain aging-associated diseases. Therefore, understanding their cellular biological properties is crucial for effective treatment development. Through traditional microscopy, lipofuscins are readily observed as fluorescent granules thought to accumulate in lysosomes. However, lipofuscin granule formation and accumulation in senescent cells are poorly understood. Thus, this study examined lipofuscin accumulation in human fibroblasts exposed to various stressors. Our results substantiate that in glucose-starved or replicative senescence cells, where elevated oxidative stress levels activate autophagy, lipofuscins predominately appear as granules that co-localize with autolysosomes due to lysosomal acidity or impairment. Meanwhile, autophagosome formation is attenuated in cells experiencing oxidative stress induced by a doxorubicin pulse and chase, and lipofuscin fluorescence granules seldom manifest in the cytoplasm. As Torin-1 treatment activates autophagy, granular lipofuscins intensify and dominate, indicating that autophagy activation triggers their accumulation. Our results suggest that high oxidative stress activates autophagy but fails in lipofuscin removal, leaving an abundance of lipofuscin-filled impaired autolysosomes, referred to as residual bodies. Therefore, future endeavors in treating lipofuscin pathology-associated diseases and dysfunctions through autophagy activation demand meticulous consideration.

Keywords: autolysosome, autophagy, cellular senescence, lipofuscin, lipofuscin granule

INTRODUCTION

Oxidative damage accumulation occurs in tissues of older adults and cells undergoing extended division *in vitro*. The gradual shift toward increased damaged adduct generation and decreased removal leads to their accumulation, which impairs body function and effectuates cellular senescence. Lipofuscins, the most prominent damage product, are oxidized lipid and protein complexes that accumulate in tissue cells with highly active energy metabolism, such as brain and cardiac muscle, and in the skin of older adults (Kwag et al., 2015; Moreno-García et al., 2018). While lipofuscin accumulation characterizes cellular and tissue aging, it is onerous for cellular function and viability. Lipofuscins induce cellular senescence and subsequent tissue aging (Porta, 2002; Singh Kushwaha et al., 2019); accumulation in the eye is a prominent macular degeneration risk factor (Julien and Schraermeyer, 2012; Wolf, 2003). In addition, lipofuscin accumulation is implicated in acromegaly, denervation atrophy, myopathies, chronic obstructive pulmonary disease, Alzheimer's disease, Parkinson's disease, amyotrophic lateral sclerosis, and other neurodegenerative disorders (Allaire et al., 2002; Moreno-García et al., 2018). Furthermore, it can induce complement activation and trigger inflammatory processes (Radu et al., 2011).

Lowering lipofuscin levels is vital for body function and

Received January 23, 2023; revised April 13, 2023; accepted May 13, 2023; published online July 13, 2023

eISSN: 0219-1032

delaying aging or certain aging-associated pathologies (Jolly et al., 2002; Terman and Brunk, 2004); therefore, developing lipofuscin suppression and removal strategies is imperative. However, our current understanding of these processes is somewhat limited. Leupeptin, a protease inhibitor, has reportedly induced lipofuscin accumulation in rats (Katz et al., 1999), but its products' authenticity has been challenged (Boulton et al., 1999). Concurrently, certain chemicals are ostensibly effective in lowering lipofuscin levels. For example, centrophenoxine is a cholinergic nootropic used for treating senile dementia that notably decreased or reversed lipofuscin accumulation in post-mitotic cells over two weeks (Terman and Welander, 1999). Recently, autophagy-mediated lipofuscin granule degradation has garnered attention. Lipofuscin potentially interferes with the autophagic process, thereby preventing cellular renewal and accumulating compromised cellular constituents. Thus, some theorize that autophagy flux impairment and lipofuscin accumulation are correlated (Brunk and Terman, 2002).

However, the association between lipofuscin accumulation and autophagy is not definitive. A recent study administering rapamycin treatment over six months reduced lipofuscin accumulation in older rat cardiomyocytes, proposing that autophagy effectively curtails lipofuscinogenesis and promotes lipofuscin degradation (Li et al., 2021). Nonetheless, autophagy activation may be better for preventing lipofuscin accumulation rather than their removal. Similarly, remofuscin reversed lipofuscin accumulation in older human retinal pigment epithelium cells and restored retinal degeneration in a pathologic Stargardt disease mouse model. Remofuscin presumably degrades lipofuscin into small particles likely removed through exocytosis, although the underlying mechanism remains inconclusive (Fang et al., 2022). Therefore, clarifying the relationship between autophagy and lipofuscin accumulation and removal is imperative.

Lipofuscins exist as granules with an approximate 1 to 5 μm diameter range within cells and are generated in a cellular organelle's lipid membrane, including lysosomes. Also known as lipofuscin granules, lipofuscin formation may develop within lysosomes through lysosomal content oxidation (Brunk et al., 1992). In lysosomes, hydroxyl radicals are potent oxidants generated through the Fenton reaction aided by Fe^{++} ions and the abundantly available oxidized lipid peroxides. Meanwhile, lipofuscin fluorescence spreading in cytosols suggests a cytosolic lipofuscin formation localization (Höhn et al., 2012; 2013). Furthermore, these free extra-lysosomal lipofuscin levels amplify upon autophagy inhibition (Höhn et al., 2012). Therefore, some lipofuscins, if not all, are created freely in cytosol from oxidized materials and captured in lysosomes before emerging as granular lipofuscins. However, the free and granular lipofuscin relationship has not yet been determined, and whether cellular stress conditions sway their measure remains unknown. This study examined lipofuscin accumulation in human fibroblasts under several conditions, including glucose deprivation, replicative senescence, and DNA damage-induced senescence.

Our previous study established that poor lysosome acidification in glucose-starved cells impairs autophagy flux (Song and Hwang, 2020), and a similar blockade reaction was also apparent in cells undergoing replicative senescence (Kang et al., 2017). The lysosomal acidity impairment in both conditions may be due to high oxidative stress levels activating the Ataxia telangiectasia mutated (ATM) protein, subsequently inhibiting the vacuolar-type ATPase (V-ATPase), a proton pump within lysosome membranes. The current study investigated the autophagic effects on granular lipofuscin accumulation by comparing lipofuscin granule levels in autophagy-modulated cells. Our results demonstrate that autophagy activation drives lipofuscin accumulation in lysosomes, but poor lysosomal acidity and lipofuscin molecule digestibility effectuates lipofuscin accumulation in autolysosomes. This study substantiates that inducing autophagy activation promotes lipofuscin granule formation.

MATERIALS AND METHODS

Cell culture and chemical treatments

Normal human fibroblasts isolated from healthy newborn foreskins were provided by Dr. Jin-Ho Chung (IRB No. H-1101-116-353 from the School of Medicine, Seoul National University, Korea) and maintained in Dulbecco's modified Eagle's medium (DMEM) (LM001-11; Welgene, Korea) supplemented with 10% fetal bovine serum (S-FBS-US-015; Serana, Australia) at 5% CO_2 and 37°C. The DMEM contained no glucose (LM001-79; Welgene) to simulate glucose deprivation. Cells were passaged at a 1:4 dilution until they stopped dividing at passage 32 to obtain a fibroblast population at replicative senescence. Fibroblasts mid-passage (between 20 and 24) were pulsed with 0.25 μM doxorubicin for 4 h and chased in fresh medium replaced every two days for chemically induced senescence. On Day 5, cells began expressing senescence phenotypes similar to previous studies (Song et al., 2005). Chemicals purchased from the following sources were used at 200 nM, 250 nM, 50 μM, 0.25 μM, 0.2 μM, and 0.5 μM doses, respectively: bafilomycin A1 from Enzo Life Science (USA) (BML-CM110-0100); Torin-1 from Biorbyt (UK) (orb146133); chloroquine (CQ; C6628), doxorubicin (D1515), and wortmannin (W1628) from Sigma-Aldrich (USA); and KU60019 from Selleckchem (USA) (S1570).

Western blotting analysis

Proteins extracted in RIPA buffer (50 mM Tris-HCl [pH 7.5], 150 mM NaCl, 1% Nonidet P-40, 0.5% sodium deoxycholate, 0.1% sodium dodecyl sulfate) supplemented with NaF, $NaVO_4$, and a protease inhibitor cocktail (P2714; Sigma-Aldrich) were separated through polyacrylamide gel electrophoresis and transferred to a nitrocellulose membrane. Membranes were blotted with primary antibodies; western blotting analysis and immunofluorescence imaging implemented antibodies against human LC3 (#2775; Cell Signaling Technology, USA) and β-actin (A5441; Sigma-Aldrich). Membranes were then incubated with horseradish peroxidase-conjugated secondary antibodies, and a SuperSignal West Femto substrate (Thermo Fisher Scientific, USA) visualized protein bands.

Immunofluorescence and confocal microscopy

Cells grown on coverslips were fixed in 3.7% paraformal-

dehyde with phosphate-buffered saline (PBS) for 20 min, permeabilized with 0.1% Triton X-100 in PBS for 15 min, blocked with 10% FBS in PBS for 2 h, and incubated with primary antibodies overnight. Antibodies against human LC3 (#2775) or Lamp1 (SC-20011; Santa Cruz Biotechnology, USA) detected autophagosomes or lysosomes, respectively. In addition, cells were washed and incubated with Alexa Fluor 488-conjugated anti-rabbit, 633-conjugated anti-mouse, 488-conjugated anti-mouse, 405-conjugated anti-mouse, 546-conjugated anti-rabbit, or 546-conjugated anti-mouse secondary antibodies (all from Thermo Fisher Scientific) for 2 h and visualized under a confocal microscope (LSM 510; Carl Zeiss, USA). Alternatively, lysosomes were directly labeled by using LysoTrakerRed (L7528; Thermo Fisher Scientific). Lipofuscins were visualized from cells grown on coverslips through confocal microscopy and autofluorescence at a 505-555 nm wavelength and photographed using a FITC filter after a 493 nm excitation. ImageJ analysis software (NIH, USA) counted puncta in the fluorescence images over 0.5 μm^2.

Determining lipofuscin and reactive oxygen species (ROS) levels through flow cytometry

Flow cytometric quantitation following the published methods measured cellular auto-fluorescence to quantify cellular lipofuscin level fluctuations (Goodwin et al., 2000; Sitte et al., 2001). Cell quantities were collected, washed in PBS, and applied to flow cytometry using a FACS Canto II cell analyzer (BD Biosciences, USA) at a 488 nm excitation and 530 nm emission. Mean cellular fluorescence values (10,000 per measurement) were normalized by untreated control (Ctl) values, and the ratio was expressed as bar graph fold changes. Cells were incubated with 50 nM dihydroethidium (DHE) (D1168; Thermo Fisher Scientific) and similarly processed to quantify cellular ROS levels.

Determining autophagic flux through flow cytometry

The CYTO-ID® autophagy detection kit (ENZ-51031-0050; Enzo Life Science) monitored autophagic flux in live cells following the manufacturer's protocol. When treatment ended, such as incubation upon glucose exposure, cells were trypsinized and stained with a CYTO-ID reagent, and the FACS Canto II (BD Biosciences) analyzed fluorescence through flow cytometry.

Lysosomal acidity measurement

Lysosensor yellow/blue DND-160 (L7545; Thermo Fisher Scientific) exhibits dual-excitation and -emission spectral peaks pH-dependently. Cells were stained with 2 μM Lysosensor yellow/blue DND-160 for 5 min, trypsinized, washed in PBS, and then measured for fluorescence in a fluorometer (Spectramax M2e; Molecular Devices, USA). The yellow/blue dual-emitted signal ratio determined relative lysosomal acidity.

Statistical analysis

Quantification was performed in all panels using two or three independent sample measurements from different experiments. Data are expressed as mean ± SD. In addition, a Bartlett test assessed variance homogeneity, and a one-way ANOVA analysis using InStat 3.06 (GraphPad Software, USA) compared intergroup mean values. A *P* value less than 0.05 was considered statistically significant.

RESULTS

Lipofuscin accumulation in glucose-starved and replicative senescent cells in autolysosomes

Upon incubation in a glucose-free medium (glucose starvation), human fibroblasts heavily promote oxidative phosphorylation to maintain energy homeostasis, generating high mitochondrial ROS levels (Song and Hwang, 2020). In this condition, cells likely activate autophagy to facilitate resource recycling; however, impaired flux hinders this process. High ROS levels attenuate V-ATPase on lysosome membranes and impair acidification, resulting in poor lysosomal hydrolysis and autolysosome accumulation (accumulated yellow puncta in Fig. 1A, Glu- [glucose-]). Autolysosomes also accumulate in fibroblasts (Fig. 2A), and lipofuscin levels surge in cells during replicative senescence (Goodwin et al., 2000; Von Zglinicki et al., 1995), indicating a close autolysosome and lipofuscin accumulation association.

Lipofuscin fluorescence levels and status in human fibroblasts were first examined under glucose starvation and replicative senescence conditions to confirm this link. Lipofuscin levels were substantially exacerbated in both cellular conditions (Glu-: Figs. 1B, 1C, and 1F; Rep Sen (replicative senescence): Figs. 2B and 2D). Interestingly, although the lipofuscin fluorescence increase was much greater under replicative senescence (Fig. 2D), lipofuscins were predominately granular in both conditions. In the lower panels of Figs. 1F and 2B, the dominant yellow puncta in the merged green lipofuscin and red lysosome fluorescence images indicates the lysosomal lipofuscin localization. Furthermore, the heavy lysosome and autophagosome co-localization in these cells convey that lipofuscins predominate in autolysosomes, and the impaired lysosome function in glucose-starved cells is partly responsible for this lipofuscin granule accumulation.

Figures 1D, 1E, and 1F (Glu-/KU labeled bars and panels) reveal that KU60019 administration during the three days of starvation inhibited ATM and partially, but significantly, improved the poor lysosome acidity and autophagy flux (Kang et al., 2017). Our previous study corroborates this observation (Song and Hwang, 2020). Notably, the treatment significantly reduced lipofuscin granule and lysosome concentrations in glucose-starved cells (Figs. 1F and 1G), proposing that, like autolysosome accumulation, lipofuscin granule escalation is largely caused by ATM-driven V-ATPase inactivation inducing poor lysosomal acidification. Similarly, KU60019 administration also substantially decreased lipofuscin granule volumes in cells undergoing replicative senescence (Figs. 2B and 2C). Meanwhile, glucose starvation did not elevate lipofuscin fluorescence levels in senescent cells (Fig. 2D, 'Ctl' vs 'Glu-' of early cell and the same senescent cell groups), indicating that impaired autolysosomal function is likely a common lipofuscin accumulation mechanism shared by glucose-starved and senescent cells.

However, impaired lysosomal acidity's involvement in replicative senescence could not be confirmed. Lysosomal acidity did not express lower levels in the tested senescent fibro-

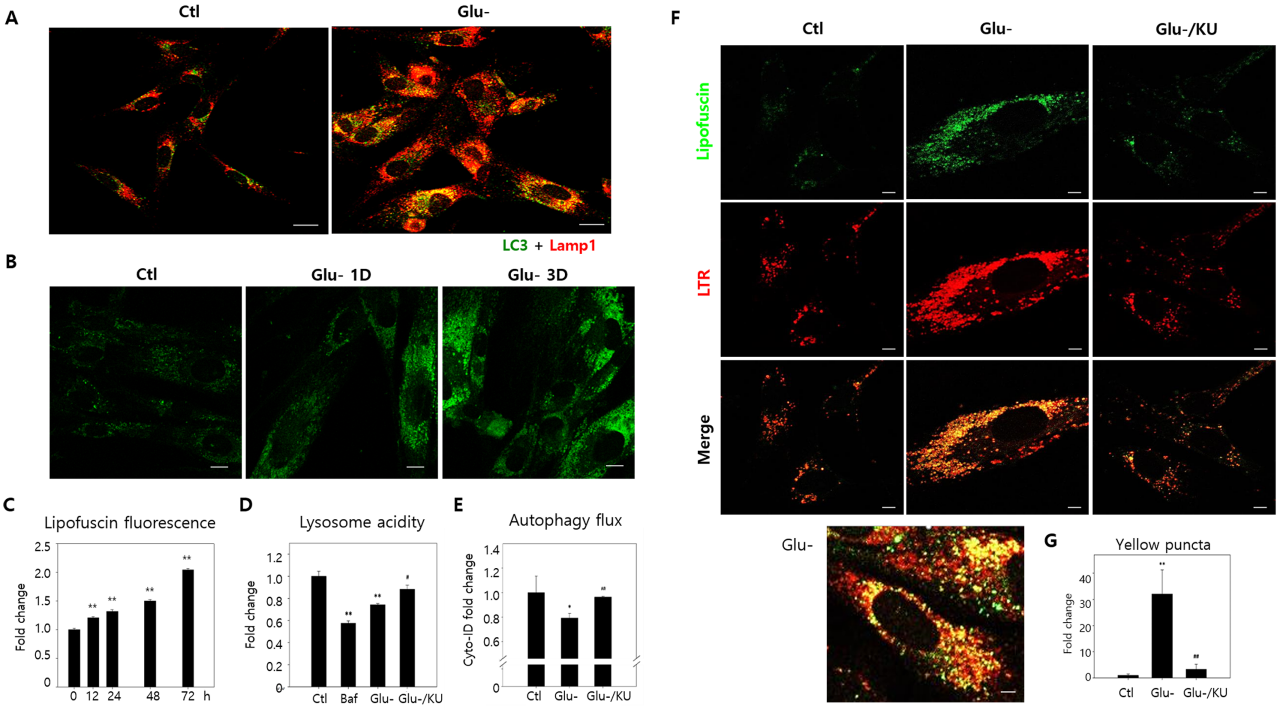

Fig. 1. Lipofuscin granule accumulation co-localized with autolysosomes in glucose-starved cells. (A) After a three-day incubation in normal (Ctl) or glucose-free (Glu-) mediums, human fibroblast immunofluorescence was measured with LC3 and Lamp1 antibodies to visualize autophagosomes (green) and lysosomes (red). Yellow puncta, representing autolysosomes, increased substantially in glucose-starved cells. (B) Confocal microscopy examined the autofluorescence of cells incubated in normal or glucose-free mediums for one (Glu-1D) or three days (Glu-3D). Granular fluorescence quantities and intensities during glucose starvation increased on Day 1, escalating further by Day 3. (C) Flow cytometry comprised 10,000 cells collected from specified times at 530 nm to determine cellular autofluorescence. Normalized data obtained through three biological repeats with the control (0 h) were plotted in the bar graph, illustrating cellular lipofuscin fluorescence differences. (D) Lysosensor yellow/blue DND-160 dye stained glucose-starved cells with or without KU60019 (Glu-/KU) for three days. After washing in phosphate-buffered saline, cells were examined through fluorometry, and relative yellow/blue fluorescence ratios determined lysosome acidity. Cells treated with 200 nM bafilomycin A1 (baf) for 1 h served as the negative control. (E) Cells were treated with 10 μM chloroquine (CQ) 24 h before collection for relative autophagy flow comparisons between glucose-starved cells with or without 0.5 μM KU60019 over three days. Cyto-ID dye stained 10,000 cells, and flow cytometry quantitated cellular fluorescence. Relative fluorescence ratios were plotted from CQ-treated and untreated cells (two biological repeats). (F and G) Lipofuscin (green) and LysoTrackRed (LTR)-stained (red) lysosome autofluorescence were visualized through confocal microscopy. Green puncta primarily overlapped with red in three-day glucose-starved cells (Glu-). The bottom panel conveys a glucose-starved cell with prominently visible yellow puncta. Meanwhile, lipofuscin and LTR puncta concentrations decreased substantially in KU60019 (Glu-/KU)-treated cells. (G) Yellow puncta (over 0.5 μm^2) were counted in ten cells from confocal photographs, and normalized control cell values were plotted. ANOVA determined $*P < 0.05$, $**P < 0.01$, $^{\#}P < 0.05$, and $^{\#\#}P < 0.01$ as significantly different. Scale bars = 20 μm.

blasts, nor was it affected by KU60019 treatment (Fig. 2E). Therefore, it remains indefinite in our experiment whether lipofuscin granule accumulation in senescent fibroblasts is minimally driven by lysosomal acidity impairment. Nevertheless, KU60019 treatment did affect lipofuscin granule levels; thus, KU60019 may affect autolysosome status independent of V-ATPase activity. Alternatively, our lysosomal acidity determination method may require further improvement to sense this slight difference significant enough to affect lysosome function.

Meanwhile, glucose-starved and senescent cells had distinct lipofuscin fluorescence and granule patterns. First, the varying 'Glu-' (early) and 'Ctl' (senescent) fluorescence levels evidenced that lipofuscin fluorescence levels were notably higher in senescent cells (Fig. 2D). Second, KU60019-treated lipofuscin granule levels exhibited no proportional change relative to lipofuscin fluorescence in both conditions. Lipofuscin granule concentrations substantially decreased in both conditions (Figs. 1G and 2C); however, the lipofuscin fluorescence attenuation was relatively small or minimal (Fig. 2C). Furthermore, enlarged replicative senescent cell images revealed green lipofuscin fluorescence that did not co-localize with lysosomal puncta (Fig. 2B, lower enlarged panel), which was not apparent in glucose-starved cells (Fig. 1F, enlarged Glu- panel). These results substantiate a potential cytosolic or non-autolysosomal lipofuscin increase in replicative senescent cells.

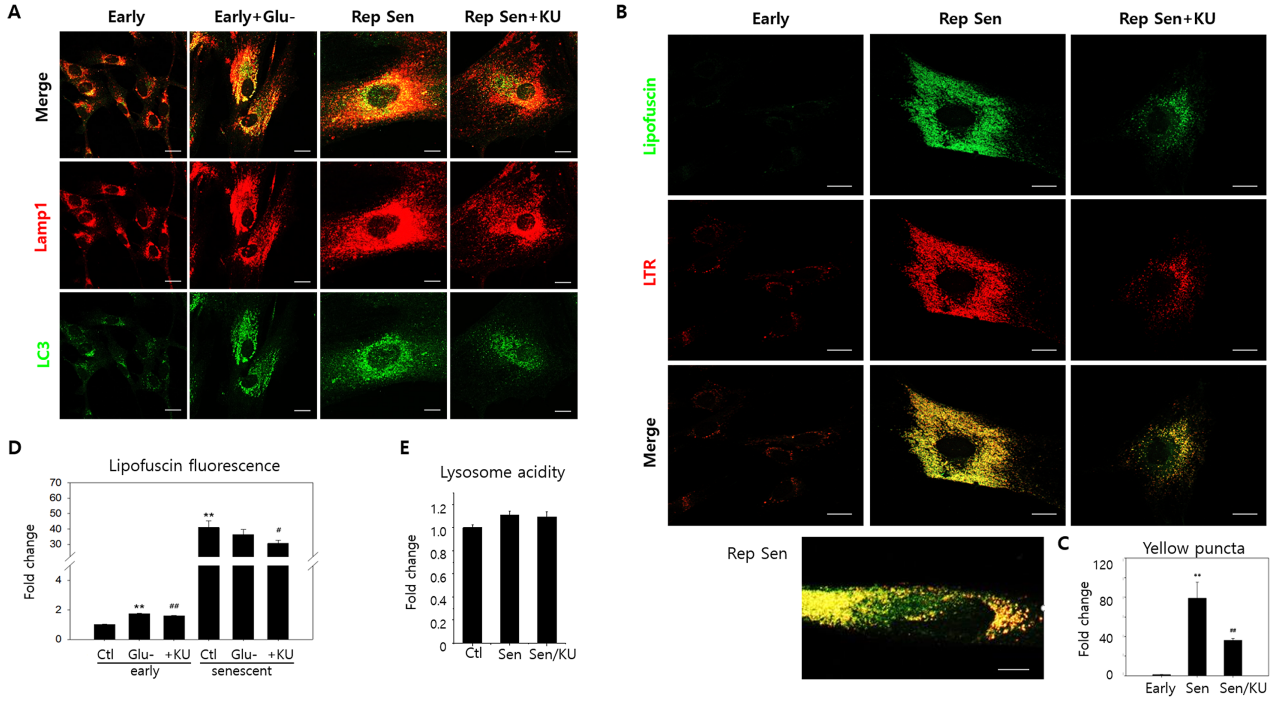

Fig. 2. Lipofuscin granule accumulation co-localized with autolysosomes in replicative senescence cells. (A) Replicative senescence human fibroblasts (passage 31 or 32) (Rep Sen) were immune-stained with LC3 autophagosomes or Lamp1 lysosomes antibodies. Compared to early-passage cells (passage 20 or earlier) (Early), Lamp1 and LC3 positive puncta were far more abundant and co-localized (yellow puncta) with a pattern similar to glucose-starved cells (Early + Glu-). KU60019 treatment for three days lowered red and green puncta levels and co-localization. (B) As visualized through confocal microscopy, autofluorescent puncta levels substantially increased and were predominantly co-localized with lysosomes in senescent cells (Rep Sen). The bottom panel illustrates senescent cells presenting granular yellow puncta and cytosolic green fluorescence. KU60019 treatment attenuated lipofuscin granule and lysosome accumulation (Rep Sen + KU). LTR, LysoTrackRed. (C) Yellow puncta (over 0.5 μm^2) were counted in ten sample cells visualized by confocal photographs, and normalized control cell values were plotted. (D) Early passage and replicative senescence cells were glucose-starved (Glu-) or treated with KU60019 (+KU). Flow cytometry examined 10,000 cells at 530 nm to determine cellular autofluorescence. Means normalized by the control were plotted (three biological repeats). (E) Early passage (Ctl) and senescent cells were either mock- (Sen) or KU60019 (Sen/KU)-treated. Lysosensor yellow/blue DND-160 dye stained 10,000 cells for lysosome acidity determination. ANOVA determined $^{**}P < 0.01$, $^{\#}P < 0.05$, and $^{\#\#}P < 0.01$ as significantly different. Scale bars = 20 μm.

Lipofuscin fluorescence increases, but lipofuscin granules are attenuated during doxorubicin-induced senescence progression

Lipofuscin levels increase in cells under oxidative stress (Sohal and Brunk, 1989), and glucose starvation and replicative senescence are prevalent alongside heightened ROS levels (Kang et al., 2006; Song and Hwang, 2020). Similarly, lipofuscin levels also increase in induced-senescent cells with high ROS levels (Cho et al., 2011; Goodwin et al., 2000). Treating cells with 0.25 μM doxorubicin for 4 h followed by chasing for five or more days has been employed as an induced senescence model. Senescence phenotypes, such as senescence-associated β-galactosidase (SA-β-gal) activity and mitochondrial ROS generation, increase slowly during the early stage, but senescence phenotype and ROS levels intensify substantially the longer cells are chased (usually over five days post-doxorubicin pulse) (Song et al., 2005). Thus, lipofuscin levels and localization in fibroblasts undergoing doxorubicin-induced senescence were closely investigated. Cellular lipofuscin fluorescence levels progressively increased, reaching a level three to four times higher by Day 6 (Fig. 3A). Although this increase is considerably smaller than that in replicative senescent cells, it is comparable or greater than the increase in glucose-starved cells over a similar duration, which was approximately two to four times more (Fig. 3B).

Importantly, there is a marked difference in lipofuscin localization patterns. Contrasting glucose-starved cells (Glu-), cells chased for five days post-doxorubicin pulse expressed poorly noticeable lipofuscin granules that rarely overlapped with lysosomes (Fig. 3C, Dox 5D). These findings suggest that lipofuscins predominantly multiply in the cytoplasm rather than in autolysosomes at an early doxorubicin-induced senescence stage. Although the reasons behind this difference are unknown, it may be due to cellular or organellar degradation rate and efficiency variations. Meanwhile, lipofuscin fluorescence appeared granular following an extended chase (Supplementary Fig. S1, lipofuscin granules in cells chased for 10 or 15 days.). Like other senescence phenotypes, lipofuscin

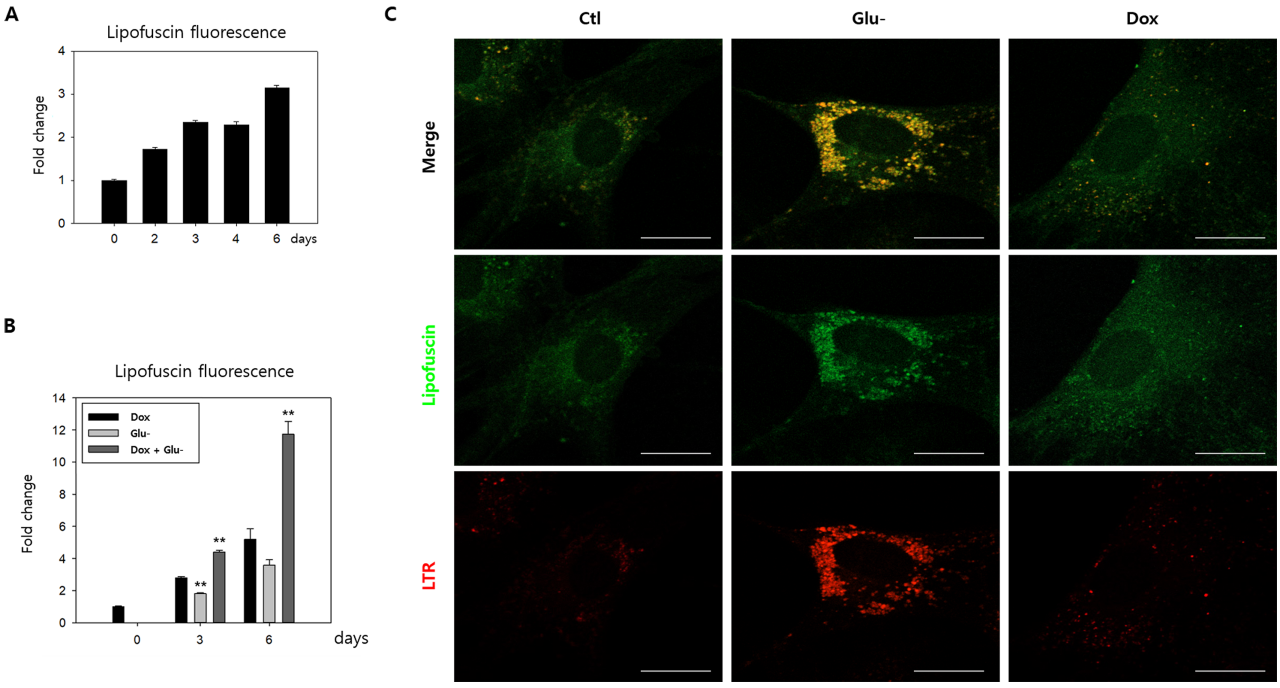

Fig. 3. Lipofuscin fluorescence primarily increased in the cytoplasm of doxorubicin-induced senescence cells. Human fibroblast senescence was induced by a doxorubicin pulse and chased for five or six days, during which flow cytometry quantified 10,000 cells for lipofuscin fluorescence (A and B) or confocal imaging assessed autofluorescence and lysosomes (stained with LysoTrackRed [LTR]) (C). (B) Lipofuscin fluorescence levels gradually increased and surpassed glucose-starved levels (pale-grey bar, Glu-) in cells chased for three or six days (black bar). Glucose starvation during the chase substantially elevated lipofuscin fluorescence (dark grey, Dox + Glu-). The three biological repeats' means were determined, and relative changes were plotted. (C) Yellow puncta were rarely visible in the cells chased for five days (Dox 5D), contrasting cells that underwent glucose starvation for three days (Glu-). ANOVA determined $**P < 0.01$ as significantly different. Scale bars = 20 μm.

granule formation potentially increases during senescence maturation. Lipofuscin fluorescence increased further when the cells were exposed to glucose starvation during the chase period (Fig. 3B, 'Dox + Glu-'), indicating that the event that takes place upon glucose starvation also occurs in senescence-induced cells and further drives lipofuscin generation. Increased ROS may be responsible for this change, but additional study is needed for confirmation.

Unlike glucose starvation and replicative senescence, autophagy activation is attenuated in cells during early doxorubicin-induced senescence stages

Many autolysosomes are prevalent when autophagy is activated in glucose starvation and replicative senescence (Figs. 1 and 2). However, only the autophagy activation molecular pathway for glucose starvation has been proposed (Song and Hwang, 2020). The low glycolysis imposed from a limited glucose supply augments the high NAD^+/NADH ratio level, consequently increasing SIRT1 activity, an NAD^+-dependent deacetylase. SIRT1 is integral to autophagy activation as it deacetylates proteins implemented in autophagy initiation, including the LC3 (Atg8) molecule that facilitates autophagosome formation (Huang and Liu, 2015). LC3 proteins are initially localized in the nucleus and released into the cytosol upon deacetylation, forming autophagosomes (Huang et al., 2015). However, autophagosomes form poorly and rarely overlap with lysosomes during early doxorubicin-induced senescence stages (chased for five days post-doxorubicin pulse), strikingly distinct from cells in other conditions (Glu-; Fig. 4A; Dox 3D and Dox 5D).

Moreover, LC3 type II molecule (LC3-II) levels, which indicate autophagosome formation, did not increase during the five-day chase in doxorubicin-induced senescence cells (Fig. 4B, left). This observation contrasts with replicative senescence cells, where LC3-II levels increased until autolysis flux was blocked by chloroquine treatment (Fig. 4B, right), indicating that autophagy is not readily activated nor is its flux blocked in induced senescence cells. Unlike cells under different conditions, where increased LC3 molecules are predominantly in the cytosol, cells doxorubicin-chased for three or five days exhibit LC3 molecules in the nucleus and perinuclear regions (Fig. 4C). These results signify that considerable LC3 concentrations are inactive and unavailable for autophagosome formation in these cells; therefore, autophagy is only marginally active or inactive in during early doxorubicin-induced senescence stages.

Autophagy activation drives lipofuscin granule accumulation during early doxorubicin-induced senescence stages

Cells chased five days following the doxorubicin pulse were

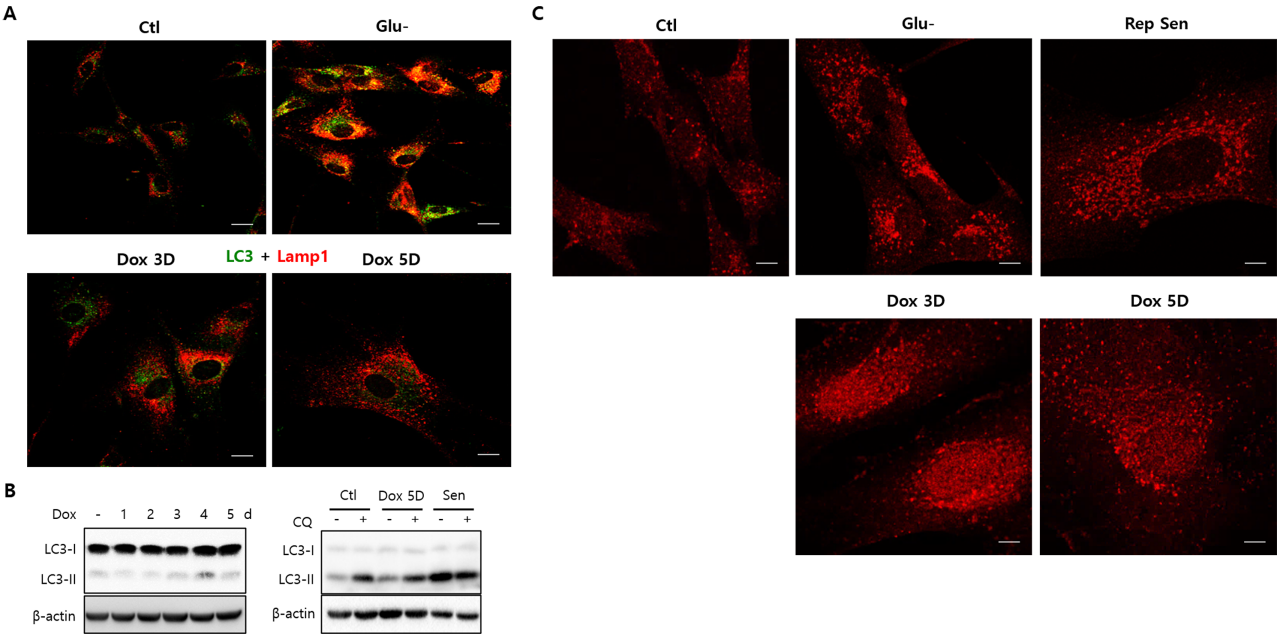

Fig. 4. Autophagy was suppressed in doxorubicin-induced senescence cells. (A) Fibroblasts chased for three or five days after doxorubicin pulse (Dox 3D and Dox 5D) were immunostained for LC3 or Lamp1. LC3-positive puncta (green) levels were low and rarely overlapped with Lamp1-positive puncta (red), indicating low autolysosome accumulation levels. This observation contrasts the high autolysosome levels in glucose-starved cells (Glu-). (B) LC3-II molecule levels did not increase during the five-day chase (upper), contrasting LC3-II levels in replicative senescence cells (Sen), where levels reached those of cells where chloroquine (CQ) treatment blocked autophagy flux (lower). (C) In cells undergoing glucose starvation for three days (Glu-) or replicative senescence (Rep Sen), LC3 molecules were exclusively localized as puncta in the cytoplasm. Alternatively, LC3 signals were abundantly localized within the nucleus and perinuclear regions in doxorubicin-chased cells (Dox 3D and Dox 5D), demonstrating an unsuccessful nuclear exit regarding the substantial LC3 molecule population. These results also indicate low autophagosome and autolysosome levels in doxorubicin-induced senescence cells are attributed to low autophagy initiation levels. Scale bars = 20 μm.

treated with Torin-1, which activates autophagy by inhibiting mTOR, to determine whether autophagy attenuation is attributable to the low-level lipofuscin granule formation (Zhao et al., 2015). Autophagy activation was verified through the LC3-II molecule increase (Fig. 5A), and Torin-1 treatment 4 h before cell collection did augment lipofuscin granules co-localized well with lysosomes (Fig. 5B, Supplementary Fig. S1). Elevated lipofuscin granule concentrations were comparable to those in glucose-starved cells (Fig. 5C). In addition, the treatment also marginally enhanced lipofuscin fluorescence levels in induced senescence cells (Fig. 5D, 'Dox' vs 'Dox + Tor'). However, lipofuscin fluorescence levels in glucose-starved cells were not notably altered by Torin-1 treatment. These results suggest that supplemental autophagy activation does not affect lipofuscin levels in cells with already accumulated lipofuscin granules, but this was not the case for cells that accumulated lipofuscin as cytoplasmic smears.

In addition, wortmannin treatment, a potent autophagy activation inhibitor (Blommaart et al., 1997), severely attenuated lipofuscin granule accumulation during the ten-day doxorubicin chase (Supplementary Fig. S2), corroborating that lipofuscin granule accumulation requires autophagy activation. Thus, these results confirm that autophagy activation is integral for granular lipofuscin formation and cellular lipofuscin elevation. Meanwhile, elevated lipofuscin granule levels from Torin-1 treatment were maintained throughout several days of examination, proposing that lipofuscin granules are autolysosomes sustaining unresolved lysosome dysfunctions or flux blockades.

DISCUSSION

Thus far, etiological events responsible for lipofuscin granule accumulation remain unknown. Therefore, this study demonstrated that lipofuscins exist as cytoplasmic smears or granules within cells, and autophagy activation accumulates autolysosomes containing lipofuscin, otherwise called lipofuscin granules. Despite previous Terman and Brunk studies (Terman and Brunk, 1998; 2004; Brunk and Terman, 2002) proposing lipofuscin granules' autolysosomal nature, how lipofuscins are trapped within autolysosomes remains largely unknown. Nevertheless, several hypotheses regarding the fate of oxidatively denatured lipid-protein complexes have emerged. Initially, these complexes were believed to remain undigested and permanently localized in lysosomes, whereas another theory considered dysfunctional excretion as a possible explanation. Notably, pigment granules, possibly lipofuscin granules, were removed from cells and phagocytosed by macrophages upon H^+/K^+ ATPase inhibitor treatment, which acidifies the cytosol (Julien and Schraermeyer, 2012). Cytosolic acidification induc-

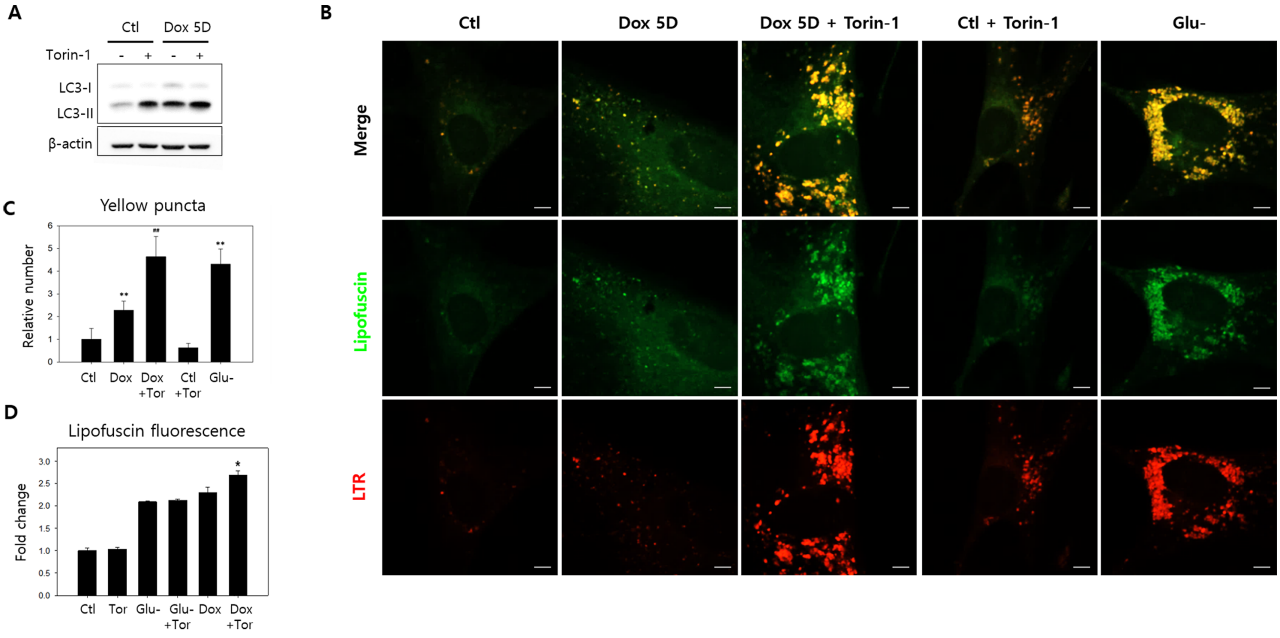

Fig. 5. Autophagy activation drives lipofuscin granule accumulation. (A and B) Fibroblasts mock-treated or chased for five days after doxorubicin pulse were treated with Torin-1 4 h before collection for LC3 molecular western blotting or confocal microscopic autofluorescence and lysosome (LysoTrackRed [LTR]) examination. (A) Torin-1 treatment increased LC3-I to LC3-II conversion, as predicted by its autophagy activation effect. (B) Treatment also increased lipofuscin granule and lysosome quantities in doxorubicin-induced senescence (Dox 5D + Torin) and control cells (Ctl + Torin). The increased lipofuscin granules primarily overlap with lysosomes, indicating autolysosomal lipofuscin accumulation. (C) Yellow puncta (over 0.5 μm^2) in the confocal microphotographs were counted in ten cells, and the average number per cell was plotted. Amounts significantly increased in cells chased for five days (Dox) and were further elevated by Torin-1 treatment (Dox + Tor) to levels comparable to glucose-starved cells (Glu-). Torin-1 treatment for control cells (Tor) did not significantly affect granule levels. (D) Lipofuscin fluorescence levels in variously treated cells were determined through flow cytometry. Torin-1 treatment alone did not affect lipofuscin fluorescence in control (Tor) or glucose-starved cells (Glu- + Tor) but significantly increased in cells chased after doxorubicin pulse (Dox + Tor), suggesting Torin-1-induced autophagy activation upregulates lipofuscin generation and granule formation. The means of the three biological repeats were plotted. ANOVA determined $*P < 0.05$, $**P < 0.01$, and $^{\#\#}P < 0.01$ as statistically different. Scale bars = 10 μm.

es a lysosomal anterograde movement to the cell periphery, facilitating lysosomal exocytosis. Although this finding does not explain how lipofuscin granules are formed, it suggests a prominent means of reducing residual bodies levels and releasing cells from the waste accumulation burden often caused by an autolysosome flux blockade.

Alternatively, lysosomal dysfunction may be driven by ROS-mediated membrane rupture or permeabilization during aging and cellular senescence (Guerrero-Navarro et al., 2022). However, this theory is not widely accepted because this response causes lysosomal enzyme leakage into the cytosol, eventually leading to necrosis. Lysosomal acidity impairment effectuates a relatively moderate lysosomal dysfunction, a more likely explanation for autolysosomal lipofuscin accumulation in oxidative stress conditions. In cells with high ROS levels, the DNA-damage response induces ATM activation, inhibiting the V-ATPase/lysosomal proton pump responsible for lysosome acidification. Comparatively, elevated mitochondrial respiration accelerates ROS production during glucose starvation, driving ATM-mediated lysosomal acidification impairment.

Additionally, oxidative stress hinders lysosomal flux, inducing a surge of lysosomes and their enzyme contents, a prominent cellular senescence phenotype (Kang et al., 2017). Although our study did not confirm whether poor lysosomal acidity influenced replicative senescence fibroblasts, it is plausible that amplified lysosomes in these conditions are autolysosomes intensified due to ROS-induced autophagy activation but impaired in cargo degradation from certain defects such as V-ATPase dysfunction. Furthermore, our study verified that ROS-mediated autolysosomal acidity impairment in glucose starvation is an etiological event in lipofuscin granule accumulation.

Still, how cytoplasmic lipofuscins localize in autolysosomes remains uncertain. Cytosolic waste is transferred to and degraded in lysosomes through macro-, chaperone-mediated (CMA), or micro-autophagy (Parzych and Klionsky, 2014). CMA specifically targets proteins, while micro-autophagy targets soluble materials. Lastly, macro-autophagy non-selectively transfers cargo in autophagosomes, inherently dependent on LC3 activation and autophagosome formation. Our results support that macro-autophagy is a likely route for autolysosomal lipofuscin localization.

Nonetheless, how autophagy activation leads to lipofuscin

granule accumulation has yet to be clarified. Another theory is that it may result from increased acidity-impaired autolysosomes, in which cargo waste becomes lipofuscins, or driven by escalated autophagic deliveries to lipofuscin lysosomes that have already formed in the cytoplasm. Our observations that lipofuscin granules dramatically increased after only a short Torin-1 treatment (4 h) suggest potential autophagosome-mediated lysosome delivery of cytosolic lipofuscins. This also eliminates the possibility that lipofuscin granules increase simply due to cell division blockage imposed by Torin-1-induced protein synthesis attenuation.

A recent study reported that increased autophagy activity helps reduce lipofuscin granule burdens in cells, proposing enhanced autophagy as a therapy for alleviating lipofuscin accumulation and associated diseases (Li et al., 2021). Li et al.'s study also concluded that rapamycin feed, another potent autophagy activator, improved lipofuscin accumulation and senescence in older rat cardiomyocytes; rapamycin treatment reduced lipofuscinogenesis while promoting lipofuscin degradation. However, our results indicate that autophagy activation contributes to lipofuscin granule accumulation. The changes observed in the study by Li et al. (2021) may not be directly caused by lipofuscin removal through rapamycin-induced autophagy. Instead, prolonged rapamycin treatment could have caused a rapid tissue turnover, thereby reducing lipofuscin granules accumulated in cells. Future studies are needed to confirm whether rapamycin treatment induces autolysosome clearance.

The possibility of SIRT1 activity impacting granular lipofuscin accumulation also requires discussion. SIRT1 is vital for health maintenance and longevity (Herranz et al., 2010). While SIRT1's involvement in lipofuscin granule accumulation and lipofuscin pathology may appear to contradict its pro-health role, SIRT1 activity declines upon aging *in vivo* (Grabowska et al., 2017; Xu et al., 2020); thus, stabilizing SIRT1 is a potential strategy for promoting healthy aging. Although SIRT1 is unlikely to be actively involved in lipofuscin pathology for aging tissues *in vivo*, caution is required for potential SIRT1 activation-induced autophagy activation effects on cells approaching senescence in aging tissues.

Note: Supplementary information is available on the Molecules and Cells website (www.molcells.org).

ACKNOWLEDGMENTS

This work was supported by the Basic Study and Interdisciplinary R&D Foundation Fund from the University of Seoul (2021-2022) granted to E.S.H.

AUTHOR CONTRIBUTIONS

S.B.S. and E.S.H. conceptualized. S.B.S. and W.S. performed formal analysis and validation. S.B.S., W.S., and E.S.H. performed data curation. E.S.H. wrote original draft preparation, review, and editing. E.S.H. secured funding acquisition and supervised.

CONFLICT OF INTEREST

The authors have no potential conflicts of interest to disclose.

ORCID

Seon Beom Song https://orcid.org/0000-0001-6497-1146
Woosung Shim https://orcid.org/0000-0002-6981-9618
Eun Seong Hwang https://orcid.org/0000-0001-8580-8444

REFERENCES

Allaire, J., Maltais, F., LeBlanc, P., Simard, P.M., Whittom, F., Doyon, J.F., Simard, C., and Jobin, J. (2002). Lipofuscin accumulation in the vastus lateralis muscle in patients with chronic obstructive pulmonary disease. Muscle Nerve *25*, 383-389.

Blommaart, E.F., Krause, U., Schellens, J.P., Vreeling-Sindelárová, H., and Meijer, A.J. (1997). The phosphatidylinositol 3-kinase inhibitors wortmannin and LY294002 inhibit autophagy in isolated rat hepatocytes. Eur. J. Biochem. *243*, 240-246.

Boulton, M., Davies, S. and Ellis, S. (1999). Lipofuscin turnover. Invest. Ophthalmol. Vis. Sci. *40*, 1887-1888.

Brunk, U.T. and Terman, A. (2002). The mitochondrial-lysosomal axis theory of aging: accumulation of damaged mitochondria as a result of imperfect autophagocytosis. Eur. J. Biochem. *269*, 1996-2002.

Brunk, U.T., Jones, C.B., and Sohal, R.S. (1992). A novel hypothesis of lipofuscinogenesis and cellular aging based on interactions between oxidative stress and autophagocytosis. Mutat. Res. *275*, 395-403.

Cho, S., Park, J., and Hwang, E.S. (2011). Kinetics of the cell biological changes occurring in the progression of DNA damage-induced senescence. Mol. Cells *31*, 539-546.

Fang, Y., Taubitz, T., Tschulakow, A.V., Heiduschka, P., Szewczyk, G., Burnet, M., Peters, T., Biesemeier, A., Sarna, T., Schraermeyer, U., et al. (2022). Removal of RPE lipofuscin results in rescue from retinal degeneration in a mouse model of advanced Stargardt disease: role of reactive oxygen species. Free Radic. Biol. Med. *182*, 132-149.

Goodwin, E.C., Yang, E., Lee, C.J., Lee, H.W., DiMaio, D., and Hwang, E.S. (2000). Rapid induction of senescence in human cervical carcinoma cells. Proc. Natl. Acad. Sci. U. S. A. *97*, 10978-10983.

Grabowska, W., Sikora, E., and Bielak-Zmijewska, A. (2017). Sirtuins, a promising target in slowing down the ageing process. Biogerontology *18*, 447-476.

Guerrero-Navarro, L., Jansen-Dürr, P., and Cavinato, M. (2022). Age-related lysosomal dysfunctions. Cells *11*, 1977.

Herranz, D., Muñoz-Martin, M., Cañamero, M., Mulero, F., Martinez-Pastor, B., Fernandez-Capetillo, O., and Serrano, M. (2010). Sirt1 improves healthy ageing and protects from metabolic syndrome-associated cancer. Nat. Commun. *1*, 3.

Höhn, A., König, J., and Grune, T. (2013). Protein oxidation in aging and the removal of oxidized proteins. J. Proteomics *92*, 132-159.

Höhn, A., Sittig, A., Jung, T., Grimm, S., and Grune, T. (2012). Lipofuscin is formed independently of macroautophagy and lysosomal activity in stress-induced prematurely senescent human fibroblasts. Free Radic. Biol. Med. *53*, 1760-1769.

Huang, R. and Liu, W. (2015). Identifying an essential role of nuclear LC3 for autophagy. Autophagy *11*, 852-853.

Huang, R., Xu, Y., Wan, W., Shou, X., Qian, J., You, Z., Liu, B., Chang, C., Zhou, T., Lippincott-Schwartz, J., et al. (2015). Deacetylation of nuclear LC3 drives autophagy initiation under starvation. Mol. Cell *57*, 456-466.

Jolly, R.D., Palmer, D.N., and Dalefield, R.R. (2002). The analytical approach to the nature of lipofuscin (age pigment). Arch. Gerontol. Geriatr. *34*, 205-217.

Julien, S. and Schraermeyer, U. (2012). Lipofuscin can be eliminated from the retinal pigment epithelium of monkeys. Neurobiol. Aging *33*, 2390-2397.

Kang, H.T., Lee, H.I., and Hwang, E.S. (2006). Nicotinamide extends replicative lifespan of human cells. Aging Cell *5*, 423-436.

Kang, H.T., Park, J.T., Choi, K., Kim, Y., Choi, H.J.C., Jung, C.W., Lee, Y.S., and Park, S.C. (2017). Chemical screening identifies ATM as a target for alleviating senescence. Nat. Chem. Biol. *13*, 616-623.

Katz, M.L., Rice, L.M., and Gao, C.L. (1999). Reversible accumulation of lipofuscin-like inclusions in the retinal pigment epithelium. Invest. Ophthalmol. Vis. Sci. *40*, 175-181.

Kwak, J.Y., Ham, H.J., Kim, C.M., and Hwang, E.S. (2015). Nicotinamide exerts antioxidative effects on senescent cells. Mol. Cells *38*, 229-235.

Li, W.W., Wang, H.J., Tan, Y.Z., Wang, Y.L., Yu, S.N., and Li, Z.H. (2021). Reducing lipofuscin accumulation and cardiomyocytic senescence of aging heart by enhancing autophagy. Exp. Cell Res. *403*, 112585.

Moreno-García, A., Kun, A., Calero, O., Medina, M., and Calero, M. (2018). An overview of the role of lipofuscin in age-related neurodegeneration. Front. Neurosci. *12*, 464.

Parzych, K.R. and Klionsky, D.J. (2014). An overview of autophagy: morphology, mechanism, and regulation. Antioxid. Redox Signal. *20*, 460-473.

Porta, E.A. (2002). Pigments in aging: an overview. Ann. N. Y. Acad. Sci. *959*, 57-65.

Radu, R.A., Hu, J., Yuan, Q., Welch, D.L., Makshanoff, J., Lloyd, M., McMullen, S., Travis, G.H., and Bok, D. (2011). Complement system dysregulation and inflammation in the retinal pigment epithelium of a mouse model for Stargardt macular degeneration. J. Biol. Chem. *286*, 18593-18601.

Singh Kushwaha, S., Patro, N., and Kumar Patro, I. (2019). A sequential study of age-related lipofuscin accumulation in hippocampus and striate cortex of rats. Ann. Neurosci. *25*, 223-233.

Sitte, N., Merker, K., Grune, T., and Von Zglinicki, T. (2001). Lipofuscin accumulation in proliferating fibroblasts in vitro: an indicator of oxidative stress. Exp. Gerontol. *36*, 475-486.

Sohal, R. and Brunk, U. (1989). Lipofuscin as an indicator of oxidative stress and aging. Adv. Exp. Med. Biol. *266*, 17-26.

Song, S.B. and Hwang, E.S. (2020). High levels of ROS impair lysosomal acidity and autophagy flux in glucose-deprived fibroblasts by activating ATM and erk pathways. Biomolecules *10*, 761.

Song, Y.S., Lee, B.Y., and Hwang, E.S. (2005). Dinstinct ROS and biochemical profiles in cells undergoing DNA damage-induced senescence and apoptosis. Mech. Ageing Dev. *126*, 580-590.

Terman, A. and Brunk, U.T. (1998). Lipofuscin: mechanisms of formation and increase with age. APMIS *106*, 265-276.

Terman, A. and Brunk, U.T. (2004). Lipofuscin. Int. J. Biochem. Cell Biol. *36*, 1400-1404.

Terman, A. and Welander, M. (1999). Centrophenoxine slows down, but does not reverse, lipofuscin accumulation in cultured cells. J. Anti Aging Med. *2*, 265-273.

Von Zglinicki, T., Nilsson, E., Döcke, W., and Brunk, U. (1995). Lipofuscin accumulation and ageing of fibroblasts. Gerontology *41* Suppl *2*, 95-108.

Wolf, G. (2003). Lipofuscin and macular degeneration. Nutr. Rev. *61*, 342-346.

Xu, C., Wang, L., Fozouni, P., Evjen, G., Chandra, V., Jiang, J., Lu, C., Nicastri, M., Bretz, C., Winkler, J.D., et al. (2020). SIRT1 is downregulated by autophagy in senescence and ageing. Nat. Cell Biol. *22*, 1170-1179.

Zhao, J., Zhai, B., Gygi, S.P., and Goldberg, A.L. (2015). mTOR inhibition activates overall protein degradation by the ubiquitin proteasome system as well as by autophagy. Proc. Natl. Acad. Sci. U. S. A. *112*, 15790-15797.